Z dependence of $4f$-$5s$ electric-octupole emission in Ag-like ions

H. A. Sakaue*
National Institute for Fusion Science, Toki, Gifu 509-5292, Japan

E. Takacs† and Dipti
National Institute of Standards and Technology, Gaithersburg, Maryland 20899, USA
and Department of Physics and Astronomy, Clemson University, Clemson, South Carolina 29634, USA

D. Kato
National Institute for Fusion Science, Toki, Gifu 509-5292, Japan
and Interdisciplinary Graduate School of Engineering Sciences, Kyushu University, Kasuga, Fukuoka 816-8580, Japan

N. Nakamura
Institute for Laser Science, The University of Electro-Communications, Tokyo 182-8585, Japan

H. Staiger
Department of Physics and Astronomy, Clemson University, Clemson, South Carolina 29634, USA

J. N. Tan
National Institute of Standards and Technology, Gaithersburg, Maryland 20899, USA

I. Murakami
National Institute for Fusion Science, Toki, Gifu 509-5292, Japan
and Department of Fusion Science, The Graduate University for Advanced Studies, SOKENDAI, Toki, Gifu 509-5292, Japan

H. Ohashi
Institute of Liberal Arts and Sciences, University of Toyama, Toyama 930-8555, Japan

Yu. Ralchenko‡
National Institute of Standards and Technology, Gaithersburg, Maryland 20899, USA

(Received 6 February 2025; accepted 31 March 2025; published 1 May 2025)

We present spectral measurements performed to identify the highly- forbidden electric-octupole ($E3$) $4f_{7/2,5/2}$-$5s_{1/2}$ transitions in Ag-like highly charged ions and to study the Z dependence of their intensities. Theoretical predictions indicate that these transitions can be observed in a narrow range of elements around tungsten ($Z = 74$), as the strong configuration interaction leads to level crossings and to an increased population of the $5s$ level. Here we probe the atomic structure and population dynamics in Ag-like ions using extreme-ultraviolet spectral measurements in several elements (Yb, Lu, W, Re, Os, Ir, Au) in the range $Z = 70$ to 79. The spectra were recorded independently in the compact electron-beam ion trap at the National Institute for Fusion Science and in the electron-beam ion trap at the National Institute of Standards and Technology. The measured wavelengths and the advanced theoretical calculations confirm observations of the $E3$ transitions in Ag-like ions in the predicted narrow element range.

DOI: 10.1103/PhysRevA.111.052801

I. INTRODUCTION

Forbidden transitions in neutral and ionized atoms have long been used in the diagnostics of solar and stellar plasmas under various physical conditions [1]. Their low radiative transition probabilities are compensated by large populations of metastable states, thereby resulting in observable spectral lines. The balance between collisional and radiative processes makes line intensity ratios sensitive to plasma parameters, particularly in low-density plasmas. Since the recognition of their diagnostic value, the importance of forbidden transitions has been extended well beyond just astrophysical observations. For instance, magnetic dipole ($M1$) lines are often used for

*Contact author: sakaue.hiroyuki@nifs.ac.jp
†Contact author: etakacs@clemson.edu
‡Contact author: yuri.ralchenko@nist.gov

the diagnostics of magnetic fusion plasmas in tokamaks and stellarators [2–4]. Recent technological advances to develop optical atomic clocks have raised great interest in spectroscopic data of higher-order multipole transitions in highly charged ions (HCIs) [5], which offer narrow linewidths and reduced sensitivity to external electromagnetic perturbations, thus resulting in highly precise and stable clocks. Furthermore, these narrow transitions could be used to search for the variation of fundamental constants and for stringent tests of fundamental physics [6–9].

Experimental studies of higher-order multipole transitions, such as the magnetic-octupole ($M3$) [10–12] and electric-octupole ($E3$) ones, are limited due to their even smaller transition probabilities. The first observation of an $E3$ transition in HCIs was reported in Ag-like tungsten ($Z = 74$) [13], connecting the $4f$ ground state to its lowest excited state $5s$. For neutral Ag ($Z = 47$) and other single-valence-electron Ag-like systems in the lower-Z part of the periodic table, the ground-state configuration is the $5s$ level, attributed to the strong correlation between the valence electron and the closed-shell core. However, with increasing Z, the relative energy of the $4f$ level rapidly decreases, approaching the natural hydrogenlike ordering of energy levels at asymptotically high nuclear charges [14,15]. This results in the crossing of the $5s$ and $4f$ levels, with the latter becoming the ground state at around $Z = 60$. The Ag-like ions near this level crossing have $E3$ transitions that lie in the optical range and have been proposed as potential candidates for the development of optical clocks and testing of fundamental constants [9,16].

Even in the early investigations motivated by magnetic fusion research, a second level crossing was observed between the $4d^{10}5d$ levels and the core-excited $4d^9 4f^2$ levels in the higher-Z elements [14,17–19]. The effect of this level crossing on the atomic data and subsequently on population dynamics suggests that the $E3$ transitions $4d^{10}4f$-$4d^{10}5s$ can be observed only in a narrow atomic number region of heavy elements in the vicinity of tungsten. The initial observation of the $E3$ decay and a discussion of the responsible physical processes were presented in [13]. In this follow-up exploration, our goal is to confirm the emission of the $E3$ lines in elements near tungsten and report their wavelengths and to investigate the Z dependence of their intensities and line intensity ratios both experimentally and theoretically. The latter poses a challenge for accurate calculations of atomic structure and kinetics, making the experiments crucial for providing benchmark results to assess the accuracy of theoretical trends.

In a collaborative effort, measurements were conducted independently at the compact electron-beam ion trap of the National Institute for Fusion Science (NIFS CoBIT) and the electron-beam ion trap at the National Institute of Standards and Technology (NIST EBIT), both equipped with state-of-the-art extreme-ultraviolet (EUV) spectrometers. The unique features of each facility and their respective detection systems contribute to the exploration of the structure and population dynamics of Ag-like systems within the region characterized by the intricate level crossings explained above. Theoretical calculations were also conducted in parallel using the General Relativistic Atomic Structure Package (GRASP) [20] and the Hebrew University Lawrence Livermore Atomic Code (HULLAC) [21]. In this paper, we describe the experimental procedures used to measure the EUV spectra in Ag-like ions of Yb, Lu, W, Re, Os, Ir, and Au; the data analysis; and the theoretical calculations performed and present our results.

II. EXPERIMENTAL PROCEDURE

Independent measurements were performed using advanced EUV spectrometers at both the compact electron-beam ion trap located at NIFS and the electron-beam ion trap at NIST. The two EBIT systems are different in the magnetic fields used to compress their electron beams in the trap region and therefore operate at considerably different electron densities. They also use different injection methods to introduce the ions of interest to the trap region. In addition, the EUV spectrometers utilize different collection geometries and transmission and detection efficiencies. The different experimental features of the two facilities allowed cross checking of the results obtained and the uncertainties assessed. The two systems were described elsewhere; however, for completeness we briefly describe them below, especially highlighting the features important for the current observations.

A. NIFS CoBIT

At NIFS, experiments were performed using a compact electron-beam ion trap, called CoBIT [22,23]. CoBIT mainly consists of an electron gun, an ion trap (drift tube), an electron collector, a superconducting coil, and a liquid-nitrogen tank. A high critical temperature superconducting Helmholtz-like coil, which can be used at the liquid-nitrogen temperature, is mounted around the drift tube. An electron beam less than 30 mA emitted from the electron gun is accelerated by an up to 2500 V potential towards the drift tube while being compressed by a 0.2-T magnetic field produced by the superconducting coil. The typical electron densities in the drift tube region of the CoBIT in the present experiments were estimated to be $1\times10^{10}\,\mathrm{cm}^{-3}$. After passing through the drift tubes, the electron beam expands and is collected by the electron collector [22,23].

Sublimated vapor of tungsten hexacarbonyl $W(CO)_6$, cyclopentadienyl rhenium tricarbonyl $(C_5H_5)Re(CO)_3$, bis(cyclopentadienyl)osmium $(C_5H_5)_2Os$, and tris(2-phenyl pyridine)iridium ($C_{33}H_{24}IrN_3$) was introduced into CoBIT through a gas-injection system for the tungsten ($Z = 74$), rhenium ($Z = 75$), osmium ($Z = 76$), and iridium ($Z = 77$) experiments, respectively. For the ytterbium ($Z = 70$), lutetium ($Z = 71$), and gold ($Z = 79$) experiments, their metal vapor was produced in a Knudsen cell and introduced to CoBIT. The electron-beam energy was adjusted to optimize the production of the Ag-like charge states of the different elements. Values of 650 eV for Yb, 715 eV for Lu, 870 eV for W, 940 eV for Re, 1000 eV for Os, 1100 eV for Ir, and 1180 eV for Au were used, in accordance with the increasing Z-dependent ionization potentials involved [24].

Radiation in the EUV region was observed with an originally designed grazing-incidence flat-field spectrometer [25] with an aberration-corrected concave grating (Shimadzu Corporation 30-002) and a back-illuminated CCD detector (Princeton Instruments PIXIS-XO:400B). A zirconium foil was placed in front of the grating to suppress the stray visible

light from the cathode of the electron gun. Since the ions in CoBIT are confined in a narrow cylindrical space (several hundred microns by 30 mm), the EUV spectrometer was designed with a slitless configuration.

Wavelength calibration was performed using a cubic polynomial derived from emission lines of highly charged Ne and Ar ions, with wavelength uncertainty primarily due to fitting errors. Sensitivity calibration included the transmittance of 150-nm aluminum and zirconium filters, grating reflectivity, CCD quantum efficiency, and photon-to-electron conversion efficiency.

B. NIST EBIT

At NIST, the EBIT facility [26] was used to create, trap, and excite highly ionized charge states of W and Re. In this facility electrons emanate from a curved-surface cathode painted with BaO_2 for enhanced electron emissivity. The electron beam can reach higher energies (up to 30 keV) and beam currents (up to 150 mA), and as a result the guiding electrodes, the drift tubes, and the collector are uniquely shaped and geometrically different from the NIFS CoBIT.

Singly charged ions of W and Re were injected into the EBIT along its vertical axis from a metal-vapor vacuum-arc ion source (MeVVA) [27]. The injection is aligned along the direction of a 2.7-T magnetic field in the trap region set by a pair of liquid-helium-cooled superconducting Helmholtz magnets in the trap region. Electron-beam-current-dependent electron densities can reach up to 10^{12} cm^{-3} in the center of the machine, leading to different trapping, ionization, and excitation conditions of the same ions compared to the NIFS CoBIT.

The optimal creation of the Ag-like charge state of these heavy elements requires around 1-keV electron-beam energy or less, like for the NIFS CoBIT. The ideal value depends on the ionization potential of the Cd-like charge state and conditions, such as the electron-beam current and the density of neutral atoms in the trap region. To maximize the number of Ag-like ions in the trap, we monitored the fairly strong $5p_{3/2}$-$5d_{5/2}$ electric-dipole EUV transition in both of these elements. Spectra were taken at different electron-beam energies and magnetic fields. The data presented here were obtained using nominal electron-beam energies of 935 and 950 eV. These values do not include corrections for the space charge of the electron beam itself [28].

For the acquisition of EUV spectra in the 2- to 18-nm region we used a slitless flat-field grazing-incidence instrument equipped with a gold-coated spherical mirror for increased solid angle of collection [29], like in several previous investigations of the NIST group (e.g., [30–32]). The main difference from the NIFS EUV spectrometer is the application of the large-area spherical mirror to increase the solid angle of collection. As a result of this extra element, there is a considerable difference between the relative efficiency curves of the two instruments, as depicted in Fig. 1.

A 100-nm-thick Zr window can be inserted in front of the spectrometer to separate its vacuum chamber from that of the EBIT and to limit the transmission of certain wavelength regions into the instrument. Spectra were taken with the Zr window both in and out in order to identify features from higher-order diffraction.

Wavelength calibration was based on known emission lines of highly charged Ne, Ar, Xe, and Ba ions. Transmission and detection efficiency were considered using an experimentally verified efficiency curve.

Due to the difference in the optical design and the geometrical arrangement of the two spectrometers, the NIST grazing-incidence instrument has a favorable energy resolution for high-precision wavelength measurements, as demonstrated by previous investigations (e.g., [32–34]). The difference in overall wavelength uncertainties reported in this paper are the result of the interplay between the different energy resolutions and the collected photon statistics.

III. DATA ANALYSIS

For the NIFS CoBIT data, the wavelength calibration was carried out by converting the CCD pixel number to the wavelength using the cubic polynomial function obtained with well-known emission lines of highly charged ions of injected Ne and Ar. The uncertainties of the wavelengths were estimated mainly from the errors in the Gaussian fitting for each emission line and the standard deviation of the residuals (deviation of the reference wavelength from the conversion curve).

A sensitivity calibration was also carried out using the transmittance of 150-nm-thick aluminum and zirconium filters, the reflectivity of the grating, the quantum efficiency of the CCD, and the conversion efficiency from the detected photon energy to the number of electrons. Figure 1 shows the wavelength dependence of the total relative correction factor as a dashed gray curve.

In the case of the NIST EBIT, at the low electron-beam energies used in the current experiment, emissions from the M-shell ions of Ba and Xe, which are natural contaminants of the EBIT with rich EUV spectral features of their own, appeared as part of the background spectrum. For the efficient removal of stronger blended features in Re we used the technique of subtracting the spectra of Os otherwise taken under identical conditions [35]. In the case of W, no such subtraction was available due to the lack of a suitable recorded spectrum; therefore, features from Ba and Xe contaminant lines appeared, especially at longer wavelengths. Background subtraction in the NIST data was done via a high-order polynomial fit of low-noise regions throughout each spectrum. Once the background was subtracted, the spectra were divided by the efficiency curve to obtain relative intensity values. Figure 1 shows spectra obtained for W and Re as thin red and blue lines for comparison with the similar NIFS CoBIT spectra. For the NIFS EBIT, there are natural contaminants that may contribute to the background signal. However, these contaminants differ from those observed in the NIST EBIT, where Ba and Xe lines were identified. While specific contaminants such as Ba and Xe were not observed in the NIFS EBIT, other species may still be present under the experimental conditions, although they were not significant enough to interfere with the measurements.

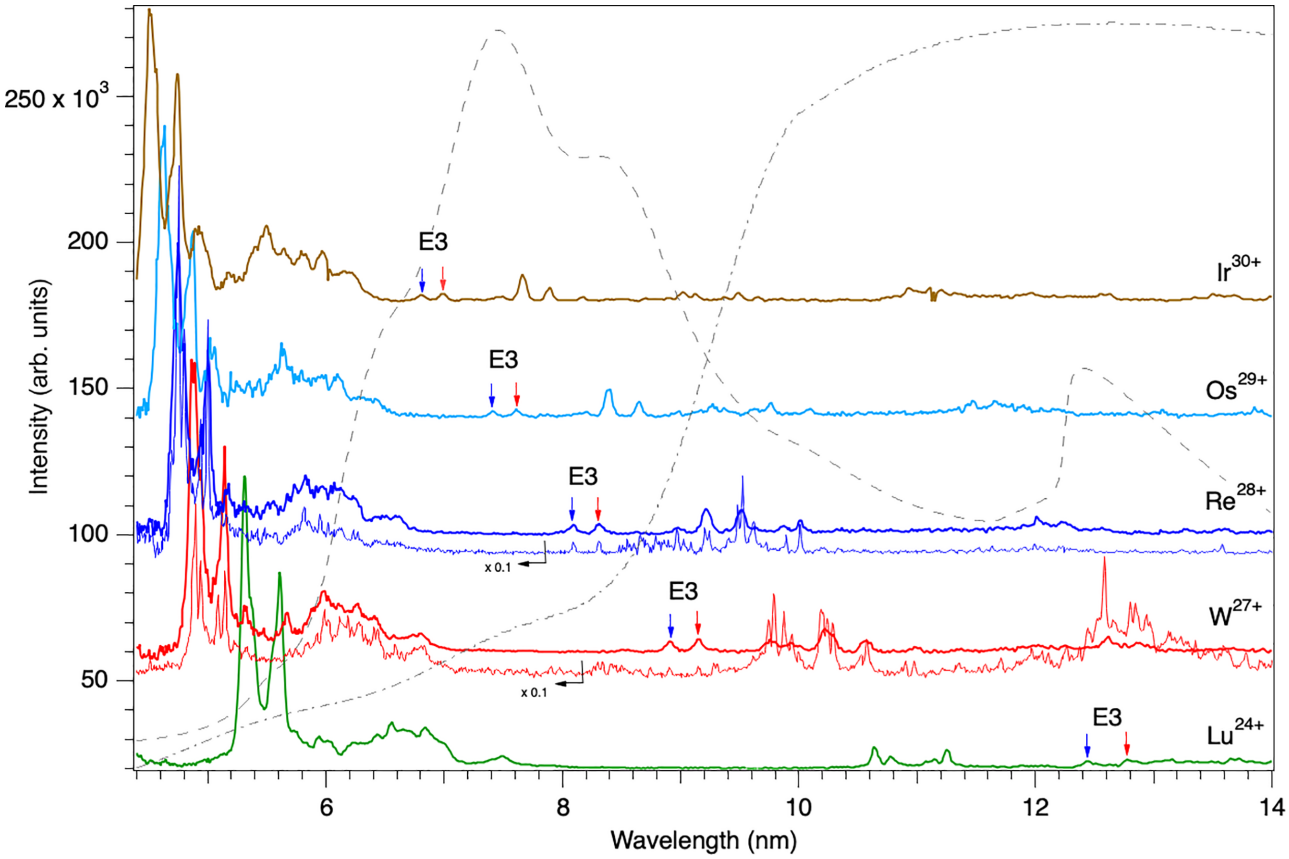

FIG. 1. Spectra of Ag-like ions measured at the NIFS CoBIT (thick lines) and at the NIST EBIT (thin lines). Relative efficiency corrections for the two systems are indicated by dashed (NIFS CoBIT) and dash-dotted (NIST EBIT) lines. The "x 0.1" labels refer to the scaling factor applied to the spectra for clarity in the plot. Arrows indicate the positions of the $4f_{5/2}$-$5s_{1/2}$ (blue) and the $4f_{7/2}$-$5s_{1/2}$ (red) $E3$ transitions. The y axis represents the relative intensity of the spectra, with the efficiency curves normalized accordingly to provide a comparison of the system efficiencies. For better readability, spectra were offset by approximately 60, 100, 140, and 170 thousand units for W, Re, Os, and Ir, respectively. Although Yb and Au spectra were measured, their spectral lines fall outside the regions of level crossings in the current experiment, resulting in no observable intensities. Therefore, their spectra are not shown.

Second- and third-order features were used as additional constraints to the third-order polynomial calibration using well-known lines [24] of injected O and Ne as well as the impurities Ar, Xe, and Ba [36,37]. Outlier detection was completed by a leave-one-out procedure, where for each spectral line, a calibration was done without that line. If any lines were inconsistent with the calibration without those lines, they were marked as outliers and removed. This process continued until all spectral lines were consistent. After identification, the regions of interest were fitted with multipeak Gaussian functions to obtain the wavelengths and their uncertainties. The reported wavelength uncertainties incorporate statistical and calibration uncertainties that include a systematic component determined from the calibration fits.

IV. THEORETICAL APPROACH

The theoretical calculations of the wavelengths and radiative rates of the $E3$ lines were carried out using the GRASP2K [20] and HULLAC [21] atomic structure packages.

The GRASP2K calculations were based on the multiconfiguration Dirac-Hartree–Fock (MCDHF) method, which starts by solving the Dirac-Coulomb Hamiltonian:

$$H_{\rm DC} = \sum_{i=1}^{N}[c\boldsymbol{\alpha}_i \cdot \boldsymbol{p}_i + (\beta_i - 1)c^2 + V_{\rm nuc}(r_i)] + \sum_{i<j}^{N}\frac{1}{r_{ij}}.$$

Here $V_{\rm nuc}(r_i) = -\frac{Z}{r_i}$ is the electron-nucleus interaction, r_{ij} is the distance between electrons i and j, $\boldsymbol{p}$ is electron momentum operator, and $\boldsymbol{\alpha}$ and β are the Dirac matrices.

Electron correlations are included by expanding the N-electron atomic state function $\psi(\gamma PJM_J)$ (where P is the parity, J and M_J are angular quantum numbers, and γ represents the additional quantum numbers required to specify the state) in the linear combination of configuration state functions (CSFs) $\phi(\gamma PJM_J)$ which are built from the antisymmetric sums of products of N single-electron Dirac spinors:

$$\psi(\gamma PJM_J) = \sum_{i=1}^{N_{\rm CSF}} b_i\phi(\gamma PJM_J).$$

The mixing coefficients b_i are obtained by diagonalizing the Hamiltonian using the self-consistent field method. Calculations were performed separately for odd-parity ($4d^{10}4f$) and

even-parity ($4d^{10}5s$) states of Ag-like ions. To consider the correlation effects for the $4f_{5/2,7/2}$-$5s_{1/2}$ transitions, the CSF space was expanded by means of single and double excitations from the $4l$ orbitals ($4s$, $4p$, $4d$, or $4f$) to active sets up to the principal quantum number $n \leqslant 8$ and orbital angular quantum number l up to 7 layer by layer. In addition to the electron correlation, the Breit interactions and leading QED contributions (self-energy and screened vacuum polarization) were included perturbatively using the relativistic configuration interaction (RCI) approach.

The transition data of the $E3$ transitions between $\psi(\gamma PJ)$ and $\psi(\gamma' P' J')$ states can be expressed in terms of the reduced matrix elements of the transition operator $\hat{T}_{E_3}$:

$$\langle \psi(\gamma PJ) \| \hat{T}_{E_3} \| \psi(\gamma' P' J') \rangle = \sum_{i,j} b_i b'_j \langle \phi(\gamma_i PJ) \| \hat{T}_{E_3} \| \phi(\gamma'_j P' J') \rangle .$$

To calculate the transition probabilities, two forms of the transition operator are used, namely, the Babushkin gauge (length) and the Coulomb gauge (velocity). Since the transition probabilities are gauge invariant [38], the differences between the two can be used to estimate the uncertainty of the computed probabilities as

$$d\mathrm{T} = \frac{|A_l - A_v|}{\min(A_l, A_v)},$$

where A_l and A_v are transition probabilities in length and velocity forms [39,40].

In HULLAC, the CSFs of the RCI calculations are constructed from solutions of the single-electron Dirac equation with a parametric potential. The parametric potential was optimized to minimize the first-order average energy of the ground-state configuration. The calculations for wavelengths and probabilities for the $E3$ transitions are performed with limited correlations which include the ground state $4d^{10}4f$; single-electron excited $4d^{10}nl$ ($n = 5-6, l \leqslant n-1$), $4d^9 4f^2$, $4d^9 4f 5l$; and doubly excited $4d^9 5l^2$, $4d^8 4f^3$, and $4d^8 4f^2 5l$ configurations. The results of the calculations and how they compare with measurements are discussed in the following section.

V. RESULTS AND DISCUSSION

Figure 1 shows the sensitivity-corrected emission spectra of Lu, W, Re, Os, and Ir observed at NIFS (thick lines) and at NIST (thin lines). Experimental spectra recorded at CoBIT were analyzed using collisional-radiative (CR) simulations described in detail in a previous publication [13]. For brevity, in the CR model calculations, the required atomic data, such as energies, transition probabilities, electron-impact excitation, and ionization cross sections, were obtained using the HULLAC code. The rates of collisional processes were determined using a δ distribution function representing the electron beam of CoBIT. For the NIST data, the lines were identified from comparisons with simulations with the CR code NOMAD [41] that used atomic data from the relativistic Flexible Atomic Code (FAC) [42]. The calculated relative intensities of the $4f_{7/2}$-$5s_{1/2}$ and $4f_{5/2}$-$5s_{1/2}$ $E3$ lines with respect to the other $E1$ transitions in Ag-like ions provided additional support for their classification. In the case of W, calculations that matched the wavelengths of previously measured $E3$ transitions [13] also confirmed the identifications. Additionally, zirconium and aluminum filters helped in some cases to clearly identify the contribution of the second-order diffraction of the strong features at shorter wavelengths. The $4f_{7/2}$-$5s_{1/2}$ and $4f_{5/2}$-$5s_{1/2}$ $E3$ transition lines were observed in the spectra of Lu, W, Re, Os, and Ir ions but not in those of Yb and Au ions.

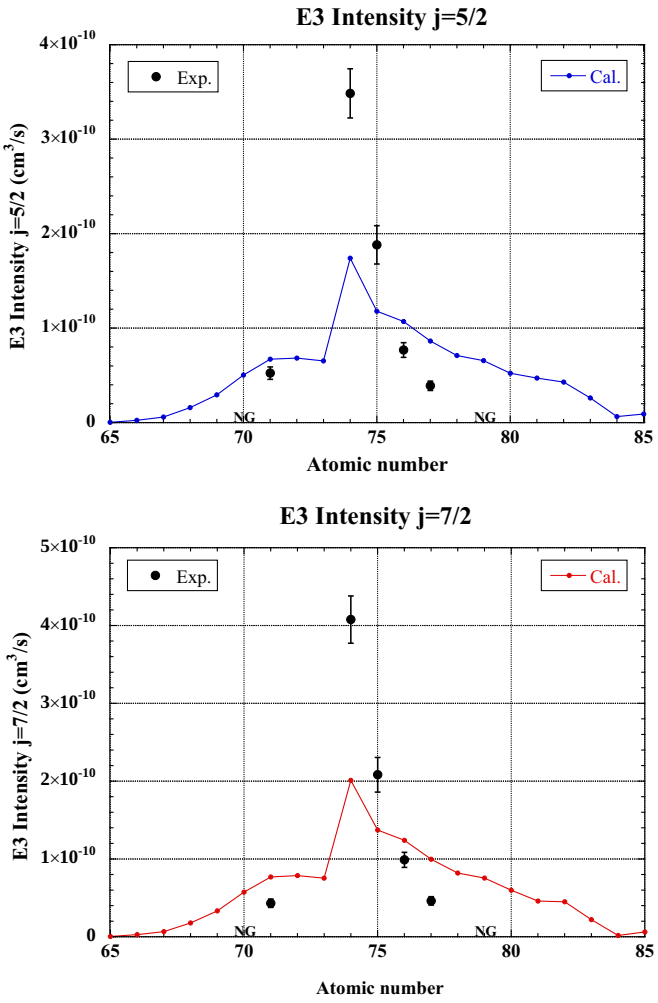

FIG. 2. The atomic number dependence of the $4f_{5/2}$-$5s_{1/2}$ and $4f_{7/2}$-$5s_{1/2}$ $E3$ transition intensities. (The error bars represent 1σ uncertainty.) "NG" indicates elements for which the intensities of the spectral lines fall to zero.

Figure 2 presents the atomic number dependence of the experimental and theoretical $E3$ transition intensity. The experimental emissivities were obtained by normalizing the intensity ratio of the $5p_{1/2}$-$5d_{3/2}$ $E1$ transition observed in the current experiment to the theoretical emissivity of the same $5p_{1/2}$-$5d_{3/2}$ transition, calculated using the CR HULLAC model. As seen in Fig. 2, the measured intensity of the $E3$ transition reaches a maximum at $Z = 74$, decreases with a further increase in Z, and is not detected at $Z = 79$. The intensity of an optically thin spectral line can be formally expressed as the product of the transition probability and population of the upper level. The strong Z dependence of the transition

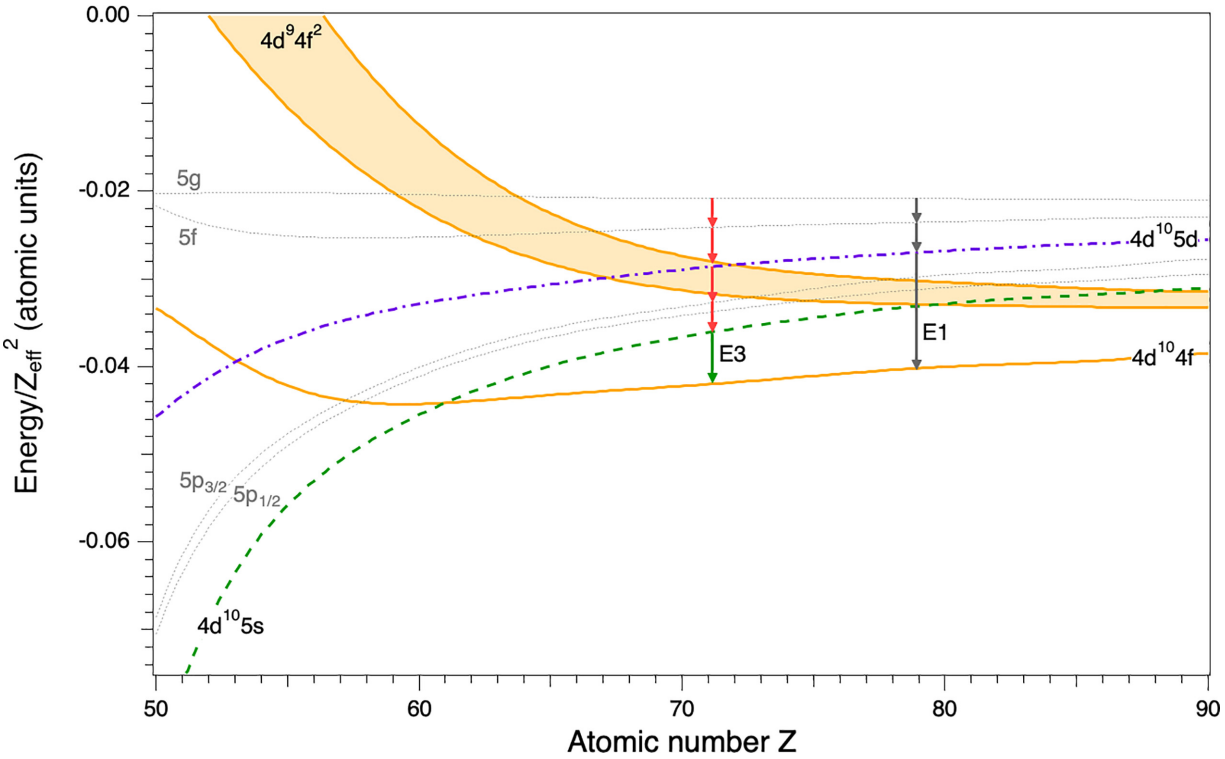

FIG. 3. Scaled term values of the lowest excited levels in Ag-like ions illustrating the level crossings of the $4d^{10}4f$ and $4d^{9}4f^{2}$ levels based on the calculations of [14]. The arrows indicate the routing of the electron deexcitation cascades near and away from the $4d^{9}4f^{2}$ level crossings. (The values presented here are expressed in atomic units, where the energy scale is in hartrees and the axis is in units of energy/$Z_{\rm eff}^2$, with the atomic number $Z_{\rm eff}^2$ being dimensionless.)

probabilities for the forbidden transitions is well established and is about Z^{40} around tungsten for the $4f_{7/2}$-$5s_{1/2}$ transition [13]. Thus, the irregularity observed in the $E3$ intensity can be explained only on the basis of an anomalous behavior of population of the $5s$ level. The population kinetics of the upper level involved were discussed in the previous work, but key details are provided here for completeness.

The population kinetics of the $5s$ level are driven by radiative cascades from the higher energy levels since the direct excitation from the ground state is negligible. As shown, e.g., in Fig. 5 of Ref. [13], the two primary population channels are due to radiative outflows from $4d^{9}nln'l'$ (mostly $4d^{9}4f5s$) and $4d^{10}5p$ levels, with the former being largely balanced by collisional excitation from $5s$. The $5s$-$5p$ radiative channel, while non-negligible, generally does not provide a significant contribution to push the $5s$ population high enough to make the $4f$-$5s$ $E3$ line intensity observable. However, as explained below, level crossings due to strong configuration mixing between $4d^{10}5d$ and $4d^{9}4f^{2}$ drastically redirect the downward population flow into the $5s$ level and thus bring about strong intensities of the $E3$ spectral lines.

Away from the level crossings, the $5d$ levels directly decay to the ground state via allowed $E1$ transitions (gray arrows in Fig. 3). In the region of the crossings between interacting states, the wave function of the $4d^{10}5d$ state is strongly mixed, with levels of the core excited $4d^{9}4f^{2}$ configuration having the same angular momenta, and can be expressed as [Eq. (1)]

$$|\Psi\rangle = b_1|4d^{10}5d\rangle + b_2|4d^{9}4f^{2}\rangle + \cdots . \quad (1)$$

The transition matrix elements of the $4d^{10}4f$ ground-state levels involve two competing terms:

$$\langle 4d^{10}4f\|\hat{T}_{E_1}\|\Psi\rangle = b_1\langle 4f\|\hat{T}_{E_1}\|5d\rangle + b_2\,\langle 4d\|\hat{T}_{E_1}\|4f\rangle. \quad (2)$$

The second term, featuring a single $4d$ hole in the core-excited configuration, can lead to cancellations or enhancements when its magnitude is comparable to that of the first term, determined by the respective signs of the terms. The minimum takes place at Z, where the primary ($4d^{10}$5d) and complementary ($4d^{9}4f^{2}$) components of the transition amplitudes cancel each other. The cancellation occurs around $Z = 74$ because the amplitude of the complementary component changes sign when passing $Z = 72$–73, and its amplitude coincides with that of the primary component around $Z = 74$. [15]. This is clearly illustrated in Fig. 4 of [13]. Thus, at this nuclear charge, the population outflux from the $5d$ level, instead of proceeding to the ground state, is routed towards the $5p$ level through the allowed $E1$ channel. The subsequent $5p \rightarrow 5s$ radiative decay greatly enhances the $5s$ population, thus giving rise to irregularity in the $E3$ intensity curve at $Z = 74$. The Z dependence of the intensity (Fig. 2) is qualitatively in good agreement with the present modeling, supporting the results of the theoretical analysis in the previous paper [13].

The wavelengths of the observed $E3$ lines are listed in Table I with theoretical values calculated using the GRASP2K and HULLAC packages. The $E3$ wavelengths measured with CoBIT and NIST EBIT are found to be in agreement within their mutual uncertainties. Overall, the GRASP2K results agree

TABLE I. Wavelengths, A values, and line intensity ratios of $4f$-$5s$ transitions in Ag-like ions. The GRASP2K A values and intensity ratios were calculated in the Coulomb (first column) and Babushkin (second column) gauges.

		Wavelength (nm)				GRASP2K A (s^{-1})		Line intensity ratio ($\frac{5}{2}/\frac{7}{2}$)				
Z	J	CoBIT	EBIT	HULLAC	GRASP2K	Coulomb	Babushkin	CoBIT	fEBIT	HULLAC	GRASP2K Coulomb	GRASP2K Babushkin
71 Lu^{24+}	5/2	12.440(9)		12.5480	12.4375	15.19	15.24	0.89(8)		0.873	0.876	0.871
	7/2	12.775(6)		12.8940	12.7770	17.35	17.50					
74 W^{27+}	5/2	8.906(6)	8.905(2)	8.9824	8.9062	87.49	87.74	0.85(4)	0.85(9)	0.865	0.868	0.863
	7/2	9.150(6)	9.142(2)	9.2253	9.1444	100.8	101.6					
75 Re^{28+}	5/2	8.089(6)	8.089(2)	8.1459	8.0919	143.1	143.5	0.90(5)	0.80(8)	0.865	0.866	0.862
	7/2	8.314(6)	8.312(2)	8.3665	8.3089	165.2	166.5					
76 Os^{29+}	5/2	7.412(5)		7.4419	7.3961	225.5	226.1	0.78(6)		0.864	0.866	0.862
	7/2	7.608(5)		7.6445	7.5954	260.5	262.4					
77 Ir^{30+}	5/2	6.803(7)		6.8364	6.7958	344.6	345.5	0.85(10)		0.866	0.866	0.862
	7/2	6.988(6)		7.0238	6.9804	398.0	400.9					

very well with the measured wavelengths. Figure 4 depicts the difference between the GRASP2K and measured values for both the $4f_{5/2}$-$5s_{1/2}$ and $4f_{7/2}$-$5s_{1/2}$ transitions. Differences between the two theories are also shown, including the Relativistic Many Body Perturbation Theory (RMBPT) calculations in [43] for W. The difference plot reveals a close (better than 0.01 nm) agreement with the GRASP2K and RMBPT results. The agreement between the HULLAC calculations and the experiments is about 0.1 nm and improves for heavier elements.

The measured wavelengths of the $E3$ transitions also provide the fine-structure splitting of the ground state $4f$, with the two levels connected by a magnetic-dipole ($M1$) transition. This transition was previously studied along the Ag-like isoelectronic sequence [19,44,45] to establish the ground state of Ag-like ions and compare atomic calculations. Our values of 334.0(120) nm and 343.5(41) nm for the $M1$ transition in Ag-like W^{27+} agree reasonably within the combined experimental uncertainties, with the previously reported precise value of 337.843(26) nm obtained through visible spectrum measurements at the Shanghai permanent magnet electron-beam ion trap [44].

Table I also includes the transition probabilities in the Coulomb and Babushkin gauges calculated from the GRASP2K

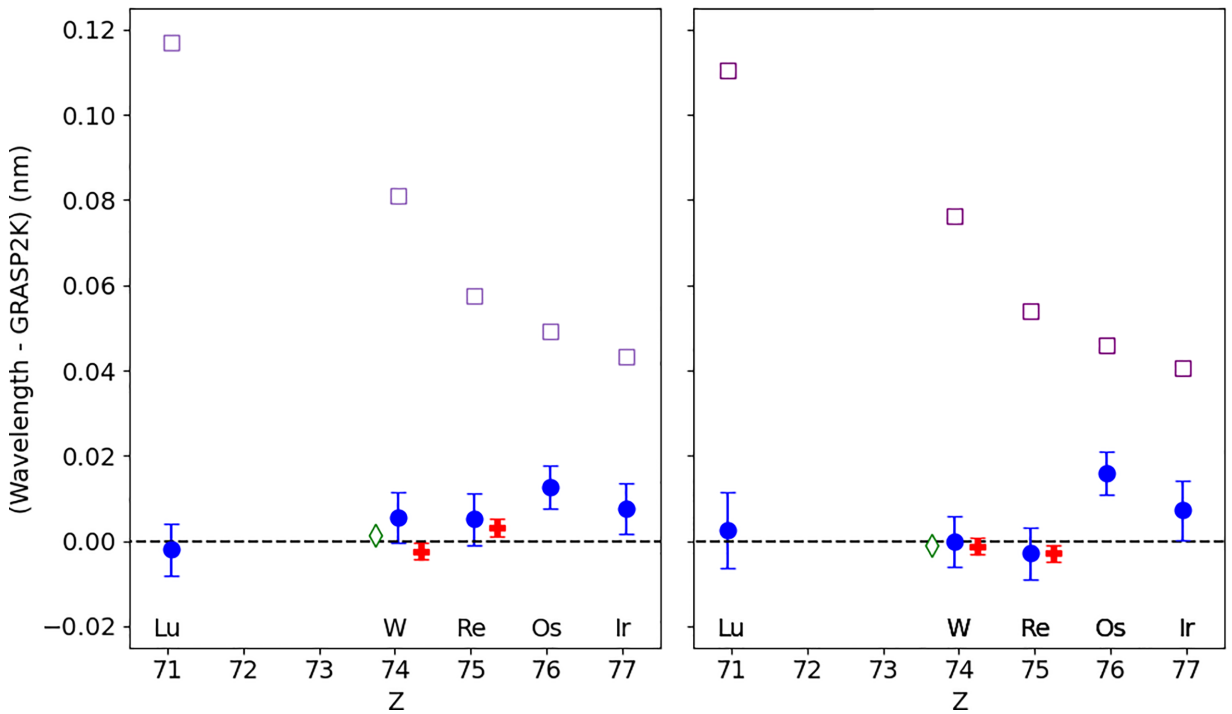

FIG. 4. Theoretical (open symbols) and experimental (solid symbols) wavelength differences with respect to the GRASP2K theoretical values for the $4f_{5/2}$-$5s_{1/2}$ (left) and $4f_{7/2}$-$5s_{1/2}$ (right) transitions. HULLAC calculations are depicted by squares, and RMBPT calculations for W [43] are depicted by diamonds. (The error bars represent 1σ uncertainty.)

code. The close agreement between the results of the two gauges is also evident from the uncertainty indicator [Eq. (1)] given in Table I. The intensity ratios of the two $E3$ lines are also listed in Table I. The ratio of the two $E3$ intensities is independent of the population mechanism of the $5s_{1/2}$ upper level; therefore, the agreement between the theoretical results and the experimentally measured values provides further confidence in the results.

VI. CONCLUSIONS

We presented detailed spectroscopic measurements and theoretical analyses to identify the $4f$-$5s$ $E3$ transitions in Ag-like ions in a narrow range of elements around tungsten. Spectra were measured using two facilities, NIFS CoBIT and NIST EBIT, with differences in their characteristics such as different electron densities, injection methods, and detection capabilities of the EUV spectrometers. The forbidden $E3$ lines were unambiguously identified in both the CoBIT and EBIT spectra through CR modeling using other $E1$ features in the Ag-like ions. The measured spectra clearly showed the presence of both the $4f_{5/2}$-$5s_{1/2}$ and $4f_{7/2}$-$5s_{1/2}$ transitions in the Ag-like ions of Lu, W, Re, Os, and Ir but not in Yb ($Z = 70$) and Au ($Z = 79$). These observations allowed us to investigate the Z dependence of the $E3$ line intensities to understand the atomic kinetics, which qualitatively agrees with the CR model predictions. In addition, the measured wavelengths and $E3$ intensity ratios were found to be in excellent agreement with the present MCDHF calculations.

ACKNOWLEDGMENTS

We thank R. Silwal, J. Dreiling, S. Sanders, A. Naing, Y. Yang, and A. Hosier for the help with the data taken at NIST. This work was partially funded by NIST Grant Award No. 70NANB20H87 and by National Science Foundation Award No. 2309273. H.S. is grateful for financial support from the NINS program of Promoting Research by Networking among Institutions and the JSPS KAKENHI (Grant No. JP21H04460).

Certain equipment, instruments, software, and materials are identified in this paper in order to specify the experimental procedure adequately. Such identification is not intended to imply recommendation or endorsement of any product or service by NIST, nor is it intended to imply that the materials or equipment identified are necessarily the best available for the purpose.

[1] G. Del Zanna and H. Mason, Solar UV and x-ray spectral diagnostics, Living Rev. Sol. Phys. **15**, 5 (2018).

[2] T. Oishi, S. Morita, D. Kato, I. Murakami, H. A. Sakaue, Y. Kawamoto, M. Goto, and the LHD Experiment Group, Identification of forbidden emission lines from highly ionized tungsten ions in VUV wavelength range in LHD for ITER edge plasma diagnostics, Nucl. Mater. Energy **26**, 100932 (2021).

[3] Yu. Ralchenko, J. D. Gillaspy, J. Reader, D. Osin, J. J. Curry, and Y. A. Podpaly, Magnetic-dipole lines in $3d^n$ ions of high-Z elements: Identification, diagnostic potential and dielectronic resonances, Phys. Scr. **2013**, 014082 (2013).

[4] B. Denne, E. Hinnov, S. Suckewer, and S. Cohen, Magnetic dipole lines in the $3s^2 3p^x$ configurations of elements from copper to molybdenum, Phys. Rev. A **28**, 206 (1983).

[5] S. King *et al.*, An optical atomic clock based on a highly charged ion, Nature (London) **611**, 43 (2022).

[6] A. Derevianko, V. A. Dzuba, and V. V. Flambaum, Highly charged ions as a basis of optical atomic clockwork of exceptional accuracy, Phys. Rev. Lett. **109**, 180801 (2012).

[7] V. I. Yudin, A. V. Taichenachev, and A. Derevianko, Magnetic-dipole transitions in highly charged ions as a basis of ultraprecise optical clocks, Phys. Rev. Lett. **113**, 233003 (2014).

[8] J. C. Berengut, V. A. Dzuba, V. V. Flambaum, and A. Ong, Optical transitions in highly charged californium ions with high sensitivity to variation of the fine-structure constant, Phys. Rev. Lett. **109**, 070802 (2012).

[9] M. G. Kozlov, M. S. Safronova, J. R. Crespo López-Urrutia, and P. O. Schmidt, Highly charged ions: Optical clocks and applications in fundamental physics, Rev. Mod. Phys. **90**, 045005 (2018).

[10] P. Beiersdorfer, A. L. Osterheld, J. Scofield, B. Wargelin, and R. E. Marrs, Observation of magnetic octupole decay in atomic spectra, Phys. Rev. Lett. **67**, 2272 (1991).

[11] E. Träbert, P. Beiersdorfer, G. V. Brown, K. Boyce, R. L. Kelley, C. A. Kilbourne, F. S. Porter, and A. Szymkowiak, Time-resolved soft-x-ray spectroscopy of a magnetic octupole transition in nickel-like xenon, cesium, and barium ions, Phys. Rev. A **73**, 022508 (2006).

[12] T. Burke, E. Takacs, Dipti, A. Hosier, G. O'Neil, J. Tan, H. Staiger, A. Naing, J. Marler, and Yu. Ralchenko, High resolution x-ray spectra of the time evolution of emission from metastable electronic states of highly charged Ni-like ions, Eur. Phys. J. D **78**, 78 (2024).

[13] H. A. Sakaue, D. Kato, I. Murakami, H. Ohashi, and N. Nakamura, Observation of electric octupole emission lines strongly enhanced by the anomalous behavior of a cascading contribution, Phys. Rev. A **100**, 052515 (2019).

[14] K. T. Cheng and Y. K. Kim, Excitation-energies and oscillator-strengths in the silver isoelectronic sequence, J. Opt. Soc. Am. **69**, 125 (1979).

[15] U. I. Safronova, I. M. Savukov, M. S. Safronova, and W. R. Johnson, Third-order relativistic many-body calculations of energies and lifetimes of levels along the silver isoelectronic sequence, Phys. Rev. A **68**, 062505 (2003).

[16] M. S. Safronova, V. A. Dzuba, V. V. Flambaum, U. I. Safronova, S. G. Porsev, and M. G. Kozlov, Highly charged Ag-like and In-like ions for the development of atomic clocks and the search for α variation, Phys. Rev. A **90**, 042513 (2014).

[17] R. C. Isler, R. V. Neidigh, and R. D. Cowan, Tungsten radiation from tokamak-produced plasmas, Phys. Lett. A **63**, 295 (1977).

[18] J. Sugar and V. Kaufman, Tokamak-generated tungsten radiation identified in Ag I isoelectronic sequence (W XXVIII), Phys. Rev. A **21**, 2096 (1980).

[19] J. Sugar and V. Kaufman, Ag-I isoelectronic sequence - wavelengths and energy-levels for Ce-XII through Ho-XXI and for W-XXVIII, Phys. Scr. **24**, 742 (1981).

[20] P. Jönsson, G. Gaigalas, J. Bieroń, C. Froese Fischer, and I. P. Grant, New version: GRASP2K relativistic atomic structure package, Comput. Phys. Commun. **184**, 2197 (2013).

[21] A. Bar-Shalom, M. Klapisch, and J. Oreg, HULLAC, an integrated computer package for atomic processes in plasmas, J. Quant. Spectrosc. Radiat. Transfer **71**, 169 (2001).

[22] N. Nakamura, H. Kikuchi, H. A. Sakaue, and T. Watanabe, Compact electron beam ion trap for spectroscopy of moderate charge state ions, Rev. Sci. Instrum. **79**, 063104 (2008).

[23] H. A. Sakaue, N. Nakamura, E. Watanabe, A. Komatsu, and T. Watanabe, Compact electron beam ion trap for spectroscopy of moderate charge state ions, J. Instrum. **5**, C08010 (2010).

[24] A. Kramida, Yu. Ralchenko, J. Reader, and NIST Atomic Spectra Database Team, NIST Atomic Spectra Database, version 5.12, 2024, https://dx.doi.org/10.18434/T4W30F.

[25] H. A. Sakaue, D. Kato, N. Nakamura, E. Watanabe, N. Yamamoto, C. Chen, and T. Watanabe, EUV spectroscopy of highly charged iron ions with a low energy compact EBIT, J. Phys.: Conf. Ser. **163**, 012020 (2009).

[26] J. D. Gillaspy, Y. Aglitskiy, E. Bell, C. M. Brown, C. Chantler, R. D. Deslattes, U. Feldman, L. Hudson, J. M. Laming, E. S. Meyer, C. A. Morgan, J. R. Roberts, F. G. Serpa, J. Sugar, and E. Takacs, First results from the EBIT at NIST, Phys. Scr. **1997**, 99 (1997).

[27] G. E. Holland, C. N. Boyer, J. F. Seely, J. N. Tan, J. M. Pomeroy, and J. D. Gillaspy, Low jitter metal vapor vacuum arc ion source for electron beam ion trap injections, Rev. Sci. Instrum. **76**, 073304 (2005).

[28] A. C. Gall, Inner shell atomic processes in highly charged Argon EBIT plasma relevant to astrophysics, Ph.D. thesis, Clemson University, 2019.

[29] B. Blagojevic, E. O. Le Bigot, K. Fahy, A. Aguilar, K. Makonyi, E. Takacs, J. N. Tan, J. M. Pomeroy, J. H. Burnett, J. D. Gillaspy, and J. R. Roberts, A high efficiency ultrahigh vacuum compatible flat field spectrometer for extreme ultraviolet wavelengths, Rev. Sci. Instrum. **76**, 083102 (2005).

[30] J. D. Gillaspy, D. Osin, Yu. Ralchenko, J. Reader, and S. A. Blundell, Transition energies of the D lines in Na-like ions, Phys. Rev. A **87**, 062503 (2013).

[31] Yu. Ralchenko, I. N. Draganic, J. N. Tan, J. D. Gillaspy, J. M. Pomeroy, J. Reader, U. Feldman, and G. E. Holland, EUV spectra of highly-charged ions $W^{54+} - W^{63+}$ relevant to ITER diagnostics, J. Phys. B **41**, 021003 (2008).

[32] R. Silwal, E. Takacs, J. M. Dreiling, J. D. Gillaspy, and Yu. Ralchenko, Identification and plasma diagnostics study of extreme ultraviolet transitions in highly charged yttrium, Atoms **5**, 30 (2017).

[33] C. Suzuki, Dipti, Y. Yang, A. Gall, R. Silwal, S. Sanders, A. Naing, J. Tan, E. Takacs, and Yu. Ralchenko, Identifications of extreme ultraviolet spectra of Br-like to Ni-like neodymium ions using an electron beam ion trap, J. Phys. B **54**, 015001 (2020).

[34] Y. Yang, Dipti, C. Suzuki, A. Gall, R. Silwal, S. Sanders, A. Naing, J. N. Tan, E. Takacs, and Yu. Ralchenko, Observations and identifications of extreme ultraviolet spectra of Ca-like to Na-like neodymium ions using an electron beam ion trap, J. Phys. B **56**, 175003 (2023).

[35] A. Hosier, Dipti, Y. Yang, P. Szypryt, G. Mondeel, A. N. Naing, J. N. Tan, R. Silwal, G. O'Neil, A. A. Lapierre, S. D. Blundell, J. Gillaspy, G. Gwinner, A. C. C. Villari, Yu. Ralchenko, and E. Takacs, Background and blended spectral line reduction in precision spectroscopy of EUV and x-ray transitions in highly charged ions, Atoms **11**, 48 (2023).

[36] H. Staiger, A. Kramida, E. Takacs, and Yu. Ralchenko, Diffraction order penalization to improve spectrometer calibrations, J. Quant. Spectrosc. Radiat. Transfer **328**, 109171 (2024).

[37] R. Silwal, Dipti, E. Takacs, J. M. Dreiling, S. Sanders, A. C. Gall, B. H. Rudramadevi, J. D. Gillaspy, and Yu. Ralchenko, Spectroscopic analysis of M- and N-intrashell transitions in Co-like to Na-like Yb ions, J. Phys. B **54**, 245001 (2021).

[38] I. P. Grant, Gauge invariance and relativistic radiative transitions, J. Phys. B **7**, 1458 (1974).

[39] C. Froese Fischer, Evaluating the accuracy of theoretical transition data, Phys. Scr. **2009**, 014019 (2009).

[40] J. Ekman, M. R. Godefroid, and H. Hartman, Validation and implementation of uncertainty estimates of calculated transition rates, Atoms **2**, 215 (2014).

[41] Yu. Ralchenko and Y. Maron, Accelerated recombination due to resonant deexcitation of metastable states, J. Quant. Spectrosc. Radiat. Transfer **71**, 609 (2001).

[42] M. Gu, The flexible atomic code, Can. J. Phys. **86**, 675 (2008).

[43] U. I. Safronova and A. S. Safronova, Wavelengths and transition rates for nl–$n'l'$ transitions in Be-, B-, Mg-, Al-, Ca-, Zn-, Ag- and Yb-like tungsten ions, J. Phys. B **43**, 074026 (2010).

[44] Z. Fei, R. Zhao, Z. Shi, J. Xiao, M. Qiu, J. Grumer, M. Andersson, T. Brage, R. Hutton, and Y. Zou, Experimental and theoretical study of the ground-state $M1$ transition in Ag-like tungsten, Phys. Rev. A **86**, 062501 (2012).

[45] R. Zhao, J. Grumer, W. Li, J. Xiao, T. Brage, S. Huldt, R. Hutton, and Y. Zou, The M1 ground state fine structure transition in Ag-like Yb, J. Phys. B: At. Mol. Opt. Phys. **47**, 185004 (2014).